ISSN (Print) 1226-1750
ISSN (Online) 2233-6656
Journal of Magnetics 24(4), 593-605 (2019) https://doi.org/10.4283/JMAG.2019.24.4.593

Selective Protection Miniature Circuit Breaker Electromagnetic Actuator Design and Dynamic Optimization

Xianbing Wang[1]*, Heyun Lin[2], Shuhua Fang[2], Xiangao Wang[1], and Jin Peng[1]

[1]*School of Electronic and Electrical Engineering, Chuzhou University, Chuzhou 239000, P. R. China*
[2]*School of Electrical Engineering, Southeast University, Nanjing 210096, China*

(Received 10 December 2018, Received in final form 17 October 2019, Accepted 23 October 2019)

This paper first proposes an electromagnetic actuator design and dynamic optimization method for selective miniature circuit breaker (SMCB), and realizes good coordination of electromagnetic actuator force and energy characteristics. Based on short delay tripping mechanism force and magnetic field model, it builds Matlab and Adams co-simulation platform, simulates and analyzes the magnetic field distribution and force energy property under different electromagnetic topological structure, and establishes the permanent magnet electromagnetic structure model. Then, it builds multi-field coupled mathematical model, and studies multi-objective dynamic optimization design for electromagnetic actuator based on quantum particle swarm algorithm. Finally, it develops the 100A miniature circuit breaker. The experimental results show that the optimized electromagnetic actuator design can effectively control the miniature circuit breaker tripping action threshold and mechanical characteristics.

Keywords : Selective miniature circuit breaker (SMCB), Electromagnetic actuator, Co-simulation design, Quantum particle swarm algorithm, Dynamic optimization

1. Introduction

In the terminal power distribution system, override tripping accident occurs in the case of cascaded matching miniature circuit breaker (MCB) short-circuit fault. This seriously impacts the continuity and reliability of power supply system. To fix this issue, the selective protection miniature circuit breaker (SMCB) low-voltage switchgear is developed. It really achieves the goal of full current range selective protection in the terminal distribution system. The key points to measure the SMCB selective protection are the capability to generate instant large output characteristics by electromagnetic actuator, the threshold to control actions by E and Cs characteristics, and the motion feature to break main contact during short-circuit. Therefore, the in-depth study of SMCB electromagnetic actuator design and dynamic optimization theory, provides the value in engineering application for miniature circuit breakers performance improvement.

In recent years, a lot of researches have been done on the electromagnetic actuator simulation optimization, motion process static and dynamic characteristics, interruption process arc characteristics, and intelligent tripping technology in low-voltage molded case circuit breaker (MCCB) and MCB. This provides the theoretical principles for SMCB further study [1-11]. Besides, SMCB structural design, interruption process arc characteristics and contact device design study is widely covered home and abroad [12-15]. Wang Qian and other scholars in Xi'an Jiaotong University [12] studied the three stages of the SMCB interruption process, and established the mathematical model and the interruption process dynamic equation, with experiments and simulations. Gong Junchang and other scholars in Shanghai Electric Apparatus Research Institute (Group) Co., Ltd. [13] analyzed the basic working principle of SMCB product structure, technical performance and selective protection. Ding Gaofeng and other scholars from Foretech Electric (Jiangsu) Co., Ltd. [14] proposed an FTB1 type SMCB structure to analyze the action characteristics of electromagnetic and operating mechanisms to achieve full current selective protection. Lu Kejun and other scholars in Shanghai Dianke Electrical Technology Co., Ltd. [15] proposed a technical solution for automatically closing contact device. It leveraged the

*Corresponding author: Tel: +86-0550-351-0959
Fax: +86-0550-351-0034, e-mail: chzuwang@163.com

rotary double breakpoint technology to achieve the higher SMCB breaking capacity. However, the current study has not touched the areas of static and dynamic iron core electromagnetic force, moving ejector pin, and the optimization of the connecting rod mechanism plane supporting end face frictional force and bearing torsion spring torsion force. These facts are the key points to impact selective protection miniature circuit breaker general performance.

This paper analyzes the magnetic field distribution and force energy characteristics under two topological structures of spring-structure and PM-structure electromagnetic actuator for SMCB by adopting ANSYS, Matlab and Adams software, and the electromagnetic actuator of PM-structure is established. Based on quantum particle swarm algorithm, the multi-objective dynamic optimization design of PM-structure electromagnetic actuator is carried out. The optimal structure parameters of the action threshold and output characteristic of PM actuator under E and C_S characteristic are optimized and established. Finally, design one 100A demo machine for testing purpose. The experimental results show that the initial jacking force of the electromagnetic actuator increases by 0.7N and the retaining force decreases by 4.3N. In the case of 1000A short circuit experimental current, the PM-structure electromagnetic actuator instantaneously detaches the main contact to achieve short-circuit short-delay characteristics.

2. SMCB Short Delay Mechanism Tripping Force Principle Analysis

The SMCB is a new switching device based on the new principle. In the case of short-circuit fault, the electromagnetic actuator detects the short-circuit current and operates the electromagnetic actuator to open the main contact and maintain at the breaking position. The auxiliary contact of the auxiliary circuit is still in the closed position, and the short circuit current is instantaneously switched from the main circuit to the auxiliary circuit, and the current-limiting operation is carried out by the current-limiting resistance of the auxiliary circuit. At this time, if the short-circuit current disappears, the electromagnetic actuator is reset, and the main contact in the main circuit is reset and closed again, so as to realize full selective protection and ensure the continuity and reliability of the power supply of the line. If the short-circuit current still exists, the auxiliary bimetallic strip of the auxiliary circuit delays for a period of time to release the operating mechanism by the motion mechanism, so that the main and auxiliary contacts are opened, and the SMCB is disconnected and the short-circuit fault current is removed.

When the short circuit current occurs in SMCB main circuit, the short time delay tripping mechanism detaches the main contact and switches to auxiliary contact. This implements the short delay protection feature. The electromagnetic actuator needs to conquer the torsion force generated by bearing torsion spring. The force analysis model is shown in Fig. 1.

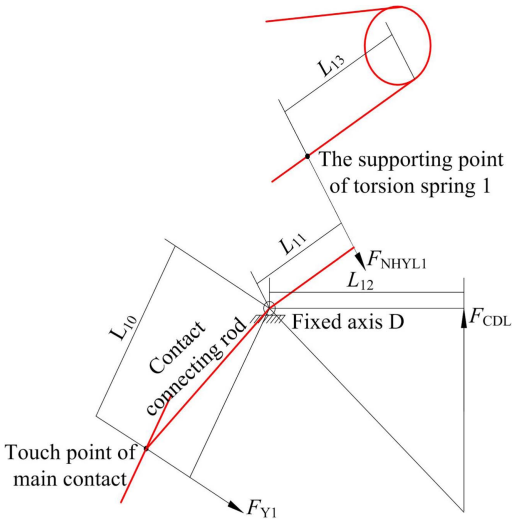

Fig. 1. (Color online) Operation force analysis model of electromagnetic actuator under initial position.

Relative to the fixed axis D, the moments of main contact end pressure F_{Y1} and bearing torsion spring pressure F_{NHYL1} are balanced. The moment formula is

$$F_{Y1} \cdot L_{10} = F_{NHYL1} \cdot L_{11} \tag{1}$$

Where F_{Y1} is the main contact end pressure; L_{10} is the force arm of fulcrum D to force F_{Y1}; F_{NHYL1} is the support arm torsion spring pressure at support point 1; and L_{11} is the force arm of the fulcrum D to the force F_{NHYL1}.

Relative to the fixed axis D, the moments of the bearing torsion spring pressure F_{NHYL1} and the initial jacking force F_{CDL} are balanced. The moment formula is

$$F_{NHYL1} \cdot L_{11} = F_{CDL} \cdot L_{12} \tag{2}$$

Where F_{CDL} is the force applied in the initial action state of the short-delay tripping mechanism; and L_{12} is the force arm of fulcrum D to F_{CDL}.

When short circuit current occurs in the miniature circuit breaker main circuit, the short delay tripping mechanism takes actions to implement the short circuit short delay feature. The short-delay tripping mechanism reaches the maximum position, and keeps the main contact in detached position. The force analysis model is shown in Fig. 2.

When the short-delay tripping mechanism reaches the maximum position, the bearing torsion spring is compressed by an angle of θ_5 from the support point 1 to

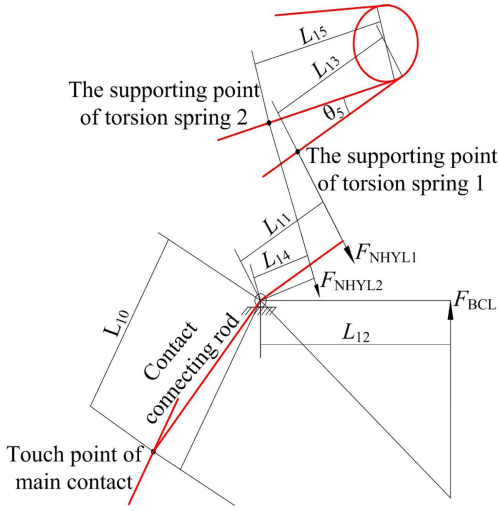

Fig. 2. (Color online) Force analysis model of electromagnetic actuator under maximum position.

support point 2. The torque generated by the bearing torsion spring is 1.8 N·mm per angle. Therefore, the torque for θ_5 is

$$T = 90 + 1.8\theta_5 \tag{3}$$

Where θ_5 is the bearing torsion spring compression angle.

When the bearing torsion spring is compressed to torsion spring support point 2, the torque balance is

$$T = F_{NHYL2} \cdot L_{15} \tag{4}$$

Where L_{15} is the force arm from the torsion spring center point to support point 2.

Relative to fixed axis D, the moment of bearing torsion springs F_{NHYL2} and F_{BCL}, with the following moment formula.

$$F_{NHYL2} \cdot L_{14} = F_{BCL} \cdot L_{12} \tag{5}$$

Where L_{14} is the force arm from axis D to support point 2 bearing torsion spring F_{NHYL2}.

3. SMCB Short Delay Tripping Mechanism Topology Structure Analysis

3.1. Electromagnetic actuator structure model

Based on the above analysis of the force principle, the fast short delay protection feature depends on the instantaneous initial jacking force and the retention on maximum position. Design the electromagnetic actuator structural model in PM structure and spring structure. Fig. 3 shows the electromagnetic actuator structural model, with Fig. 3(a) for PM structure, and Fig. 3(b) for spring structure. The PM structure electromagnetic actuator model

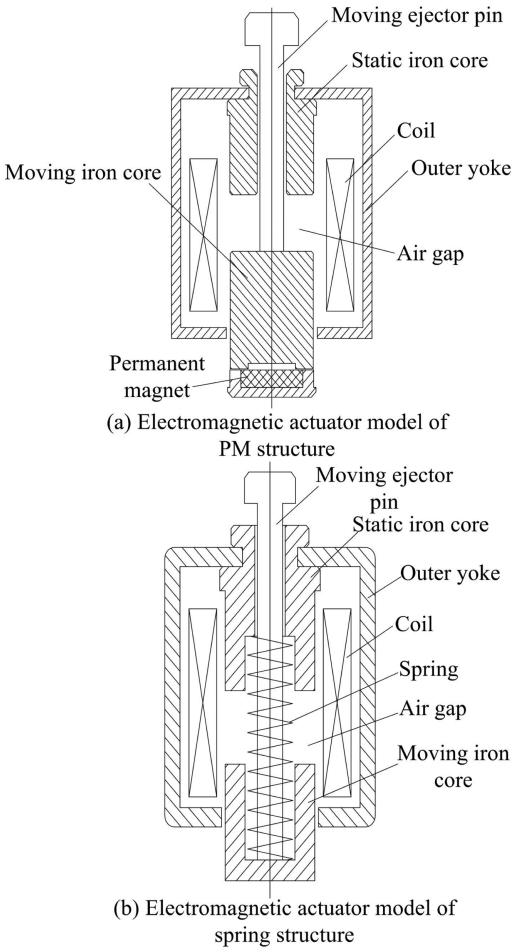

Fig. 3. Electromagnetic actuator model.

includes one moving iron core, one static iron core, one PM, one coil, one outer yoke, and one moving ejector pin. The PM is placed at the bottom of the moving iron core, and one end of the moving ejector pin is fixed at the end surface of the moving iron core. The action threshold point under the E and C_S characteristics of the electromagnetic actuator is controlled by the PM constant suction. When the short-circuit current occurs, the electromagnetic force generated by the coil is greater than the PM suction force. The moving iron core drives the moving ejector pin to take action, and implement selective protection by fast main contact detach.

The spring-structure electromagnetic actuator model includes one moving iron core, one static iron core, one spring, one coil, one outer yoke and one moving ejector pin. The spring is placed in the static and dynamic iron core slot and attached in the moving ejector pin. One end of the moving ejector pin is fixed on the bottom end surface of the moving iron core, and the other end is fixed on the bottom end surface of the static iron core. This structure controls the action threshold point under the E

and C_S characteristics via the initial spring force. When a short-circuit fault occurs, the short circuit current flows through the coil. When the electromagnetic force generated by the coil is greater than the spring force, the moving iron core drives the moving ejector pin to move the contact rod mechanism to reach detach the contact link structure, thus implements the selective protection by fast main contact detach.

3.2. Electromagnetic actuator magnetic field calculation and analysis

The electromagnetic actuator shown in Fig. 3 is a two-dimensional axisymmetric structure model, ignoring eddy current and hysteresis characteristics. Meanwhile, the PM processing is done by direct discrete method, and the nonlinearity of iron core is calculated by Newton-Raphson iterative solution. The vector magnetic potential $\boldsymbol{A}$ is used to analyze the two-dimensional static electromagnetic field, which satisfies the following nonlinear equation.

$$\begin{cases} \nabla \times \nu(\nabla \times \boldsymbol{A}) = \boldsymbol{J} & \text{in } \Omega_s \\ \nabla \times \nu(\nabla \times \boldsymbol{A} - \boldsymbol{B}_r) = 0 & \text{in } \Omega_m \\ \boldsymbol{A} = 0 & \text{on } \Gamma_1 \end{cases} \tag{6}$$

Where $\boldsymbol{J}$ is coil current density; ν is reluctivity; $\boldsymbol{B}_r$ is PM remanent flux density; Ω_m Ω_m is PM region; Ω_s is non-PM region.

When simplified to two-dimensional axisymmetric field analysis, the boundary value problem to solve the circular cross section electromagnetic actuator magnetic field is

$$\begin{cases} \Omega : \dfrac{\partial}{\partial z}\left(\dfrac{1}{\mu}\dfrac{\partial A_\theta}{\partial z}\right) + \dfrac{\partial}{\partial r}\left(\dfrac{1}{\mu}\dfrac{\partial A_\theta}{\partial r}\right) = -J_\theta \\ \Gamma_1 : A_\theta = A_0 \end{cases} \tag{7}$$

Where J_θ is coil θ direction current density; μ is magnetic permeability.

After obtaining the magnetic field distribution and the boundary value problem of the miniature circuit breaker electromagnetic actuator, the vector magnetic potential can be solved. The magnetic flux density $\boldsymbol{B}$ in the field can be further determined by $\boldsymbol{A}$.

$$\boldsymbol{B} = \nabla \times \boldsymbol{A} \tag{8}$$

In path l, the coil flux linkage ψ is obtained as

$$\psi = N \int_l \boldsymbol{A} d\boldsymbol{l} \tag{9}$$

The electromagnetic attraction of the moving iron core by the stress tensor $\boldsymbol{T}$ is represented as

$$\boldsymbol{F} = \oint_s (\boldsymbol{T} \cdot \boldsymbol{n}) dS = \oint_s \left[(\boldsymbol{B} \cdot \boldsymbol{n}) \boldsymbol{H} - \frac{1}{2} BH\boldsymbol{n} \right] dS \tag{10}$$

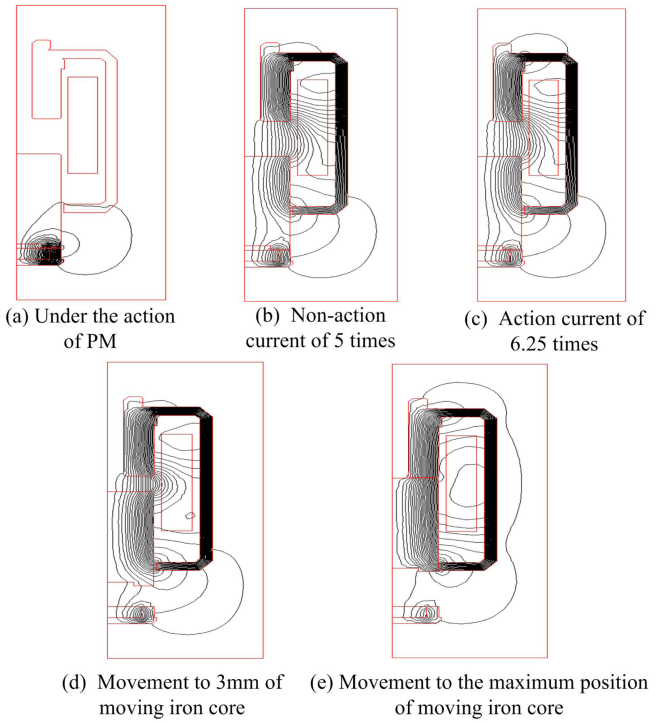

Fig. 4. (Color online) Magnetic field distribution of PM structure electromagnetic actuator.

Where $\boldsymbol{T}$ is magnetic field tension; $\boldsymbol{n}$ is dS panel unit normal vector; S is the face surrounding the moving iron core.

Fig. 4 shows the PM structure electromagnetic actuator magnetic field distribution at different positions and currents. Fig. 4(a) shows the magnetic field distribution under the action of PM alone. The magnetic lines of force are distributed in the low-end PM part, and the PM attraction is −16.18 N, as the downward suction force. The constant suction of the PM ensures the action threshold point under the E and C_S characteristics of the electromagnetic actuator. Fig. 4(b) shows the distribution of the magnetic field under the action of 5 times non-operation short-circuit current. The PM and the electromagnetic coil have the combined force of −4.2 N. When the short-circuit current is 5 times to the rated current, the force is still downward. It keeps the electromagnetic actuator 5 times non-operating characteristic, as the sum of the bearing torsion spring force and the main contact end pressure cannot be overcome. Fig. 4(c) shows the magnetic field distribution of the coil through 6.25 times action short-circuit current. The PM and the electromagnetic coil have combined force of 1.2 N. When the short-circuit current is 6.25 times to the rated current, the force exerts an upward suction force, and the moving iron core starts to move under the upward force, thereby maintaining the

operating characteristic of the electromagnetic actuator in 6.25 times current. Fig. 4(d) shows the magnetic field distribution when the moving iron core is moved to 3 mm and short-circuit current is switched to the auxiliary contact. When the PM and the electromagnetic coil have combined force of 18.6 N, the short-circuit current is switched to the auxiliary contact. The common force of the PM and the electromagnetic coil can continue to move the moving iron core upward. Fig. 4(e) shows the magnetic field distribution at the moving iron core maximum position. The PM loses its function, the electromagnetic coil force is 109.6 N. The short-circuit current is switched to the auxiliary contact, and the electromagnetic coil force keeps the main contact in the off position.

Fig. 5 shows the spring-structured electromagnetic actuator magnetic field distribution at different positions and currents. Fig. 5(a) shows the magnetic field distribution under the action of 5 times non-operation short-circuit current. The suction force between the moving and static iron core is 3.1 N. The force of the electromagnetic coil is less than the reaction force 4.5 N of the spring. The force is downward suction, and the sum of the bearing torsion spring force and the main contact end pressure cannot be overcome, thereby keeping the electromagnetic actuator 5 times non-operating characteristics. Fig. 5(b) shows the coil magnetic field distribution through a 6.25 times action short-circuit current. The suction force between the moving and static iron core is 5.16 N. The force of the electromagnetic coil is greater than the spring reaction force 4.5 N. The electromagnetic coil and the spring have combined force of 0.66 N, which is upward suction, and the moving iron core starts to move under the upward force, thereby maintaining 6.25 times the operating characteristics of the electromagnetic actuator. Fig. 5(c) shows short circuit current magnetic field distribution, switched to the auxiliary contact current limit when the moving iron core is moved to 3 mm. At this time, the force is 10.1 N. When the short-circuit current is switched to the auxiliary contact, the force generated by the electromagnetic coil can continue to move the moving iron core upward. Fig. 5(d) is the magnetic field distribution at the maximum position of the moving iron core. The force of the electromagnetic coil is 76.9 N. When the short-circuit current is switched to the auxiliary contact, the force generated by the electromagnetic coil keeps the main contact in the off position.

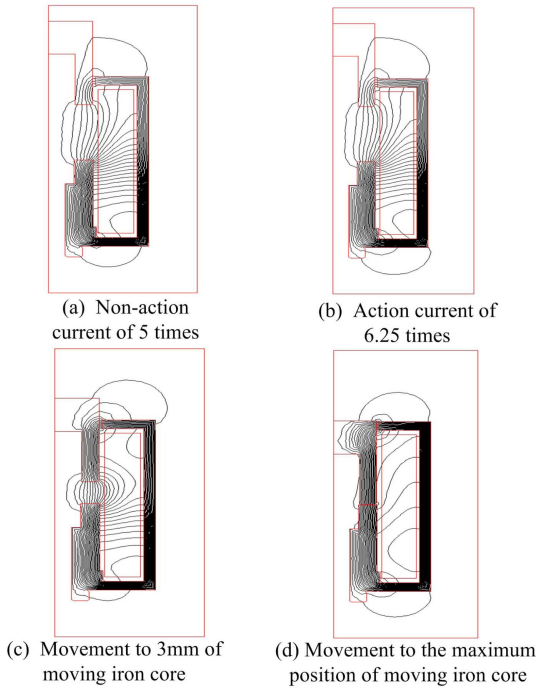

Fig. 5. (Color online) Magnetic field distribution of spring-structure electromagnetic actuator.

Fig. 6 shows the suction and reaction force characteristics curve of the electromagnetic actuator of the PM structure. The PM suction is large at the initial position, which is 5 times to the electromagnetic actuator non-operating current. When the electromagnetic force generated by the short-circuit current via the electromagnetic coil is greater than the PM suction force, the moving iron core is moved. With the movement of the moving iron core, the reaction force generated by the PM gradually loses its effect. At this time, the electromagnetic force generated by the coil acts on the moving iron core and the resultant force is above the reaction force. The electromagnetic suction force is gradually increased, and the maximum value can reach 120 N, ensuring that the moving ejector pin can detach the main contact.

Fig. 7 shows the suction and reaction force characteristics curve of the spring-structured electromagnetic actuator. The spring reaction force is large at the initial position, which is 5 times to the non-operating current of the electromagnetic actuator. When short circuit current flows through the electromagnetic coil and the electromagnetic force generated by the coil is greater than the spring reac-

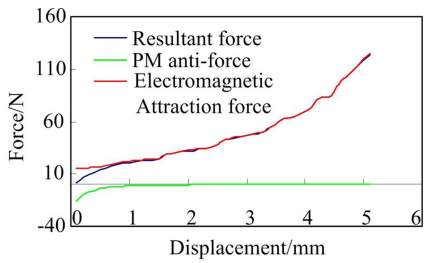

Fig. 6. (Color online) Attraction and anti-force characteristics of PM structure electromagnetic actuator.

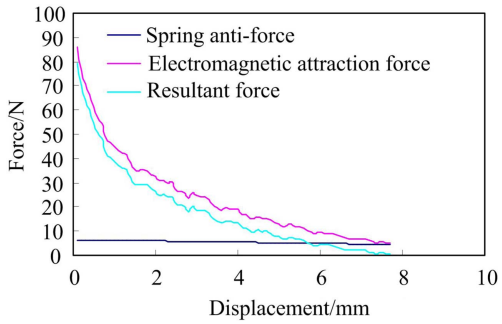

Fig. 7. (Color online) Attraction and anti-force characteristics of spring-structure electromagnetic actuator.

tion force, the moving iron core is moved. The process of the spring force for the spring structure is gradually increased, relative to the process in which the reaction force of the PM is gradually reduced. At this time, the electromagnetic force generated by the electromagnetic coil acting on the moving iron core needs to overcome larger spring reaction, ensuring that the moving ejector pin can detach the main contact.

3.3. Updated electromagnetic actuator structural parameters magnetic field calculation and analysis

3.3.1. Updated Moving Iron Core Structural Parameters Magnetic Field Calculation and Analysis

The structure change analysis of the moving iron core of the PM structure electromagnetic actuator is shown in Fig. 8. Fig. 8(a) is the analysis chart of the moving iron core height change, and Fig. 8(b) is for the moving iron core radius change. Fig. 8(a) shows that the initial height of the moving iron core is 13.6 mm. When it is increased to 15.6 mm, the suction force between the moving and static iron core gradually increases with the decrease of the air gap. When it is reduced to 11.6 mm, the suction force of the moving iron core suddenly appears to a minimum value at the 4.6 mm air gap, with the electromagnetic force 59 N. When the height of the moving iron core is low, the leakage magnetic flux between the moving iron core and the outer yoke support frame branch increases, which may cause short-delay protection failure of the short-circuit instant. Fig. 8(b) shows when the radius of the moving iron core is increased by 0.45 mm, the suction force generated by the moving and static iron core slightly increases, and when the radius of the moving iron core is decreased by 0.45 mm, the suction force generated by the moving and static iron core tends to decrease.

Fig. 9 shows the structural change analysis of the spring-structure electromagnetic actuator moving iron core. Fig. 9(a) is the analysis chart of the moving iron core height change, and 9(b) is for the moving iron core radius change. Fig. 9(a) shows that the initial height of the moving iron core is 11.6 mm. When it is increased to 13.6 mm, the suction force of the moving and static iron core gradually increases with the decrease of the air gap. When it is reduced to 9.6 mm, the moving iron core suction force is reduced to 21 N at the 1.2 mm air gap. Therefore, if the

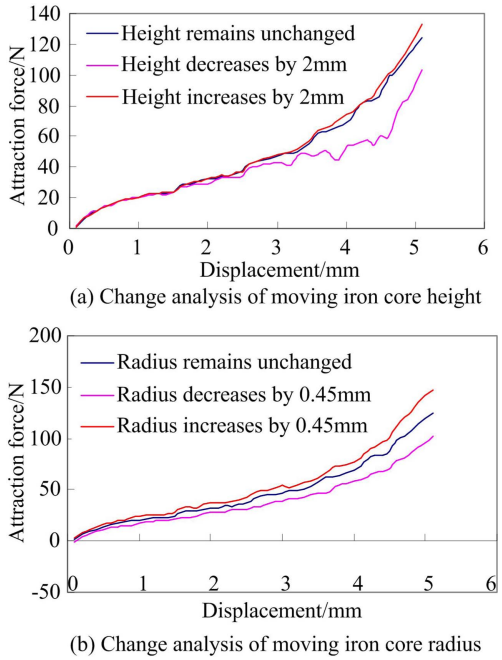

Fig. 8. (Color online) The moving core structure change analysis of PM structure electromagnetic actuator.

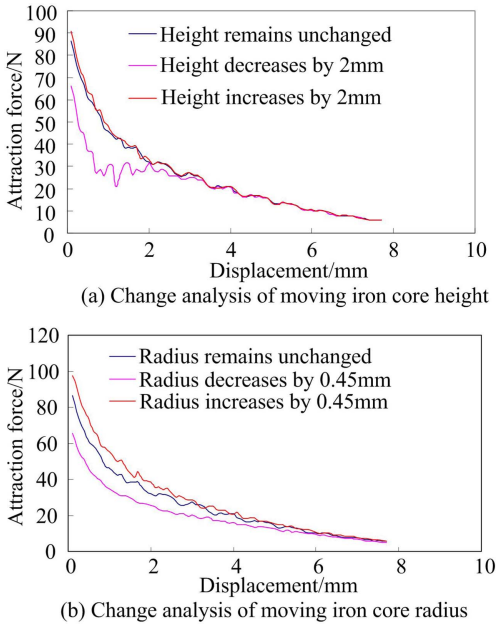

Fig. 9. (Color online) The moving core structure change analysis of spring-structure electromagnetic actuator.

height of the moving iron core plus the height of the air gap between the moving and the static iron core is smaller than the height of the lower end surface of the outer yoke support frame to the lower end surface of the static iron core, the magnetic flux leakage between the moving iron core and the outer yoke support frame branch increases, and the increase causes a sudden occurrence of a minimum value of the electromagnetic force, which may cause a short delay protection failure of the short circuit instant, and damage the SMCB main contact mechanism. Fig. 9(b) shows that the radius of the moving iron core is increased or decreased by 0.45 mm, the suction force slightly increases or decreases.

3.3.2. Updated Static Iron Core Structural Parameters Magnetic Field Calculation and Analysis

Fig. 10 shows the structural change analysis of the PM structure electromagnetic actuator static iron core.

Fig. 10(a) is the analysis diagram of the static iron core height variation. The initial height of the static iron core is 7.3 mm. When it is increased to 9.3 mm or decreased to 5.3 mm, the electromagnetic attraction between the moving and static iron cores keeps no change. Fig. 10(b) shows the static iron core radius change. When the static iron core radius is increased by 0.45 mm, the suction force generated by the moving and static iron core slightly increases. When the static iron core radius is decreased by 0.45 mm, the suction force generated by the moving and static iron core tends to decrease remarkably.

Fig. 11 shows the analysis of the spring-structure electromagnetic actuator static iron core structure change. Fig. 11(a) is the analysis diagram of the static iron core height variation. The initial height of the static iron core is 12 mm. When it is increased to 14 mm, the suction force of the moving and static iron core gradually increases with the decrease of the air gap. When it is reduced to 10 mm, the magnetic flux leakage occurs between the upper end portion of the moving iron core and the outer yoke. The increase in leakage flux causes a sudden drop in electromagnetic attraction between the moving and static iron cores at the 0.8 mm air gap, which is reduced to 21.3 N. This will cause the moving ejector pin incapability to instantly detach the miniature circuit breaker main contact. Fig. 11(b) shows the static iron core radius change. When the radius of the static iron core is increased or decreased by 0.45 mm, the suction force generated slightly increases or decreases.

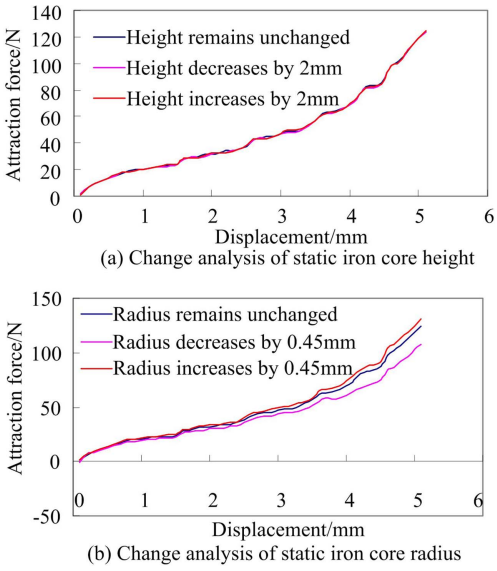

Fig. 10. (Color online) The static core structure change analysis of PM structure electromagnetic actuator.

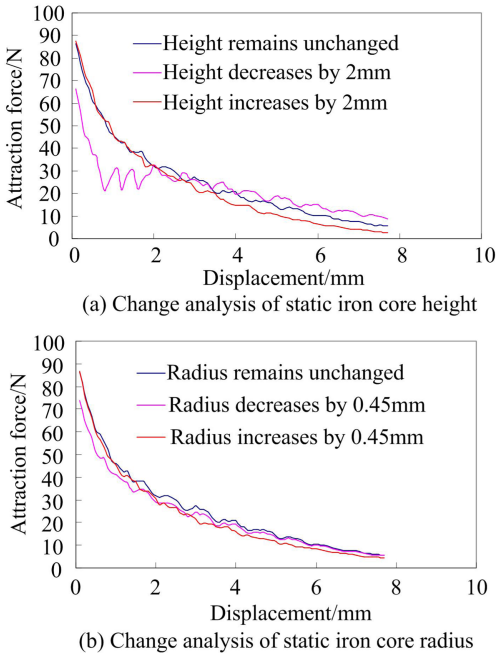

Fig. 11. (Color online) The static core structure change analysis of spring-structure electromagnetic actuator.

3.3.3. Updated Outer Magnetic Yoke Width Parameter Magnetic Field Calculation and Analysis

Fig. 12 shows the variation of the outer yoke width parameter of the electromagnetic actuator. Fig. 12(a) is the change analysis of the PM structure electromagnetic actuator outer yoke width parameter, and Fig. 12(b) is for spring-structure. Fig. 12(a) shows when the outer yoke width is increased by 0.45 mm, the suction force generated by the moving and static iron core has no significant change, and when the outer yoke width is reduced by 0.45 mm, the suction force generated by the moving and

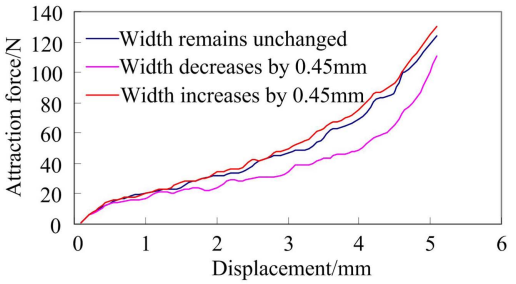

(a) Width change analysis of the outer magnetic yoke of electromagnetic actuator for PM structure

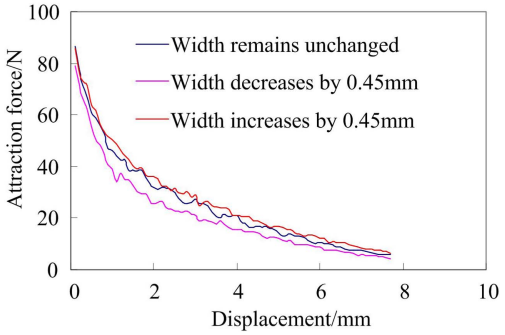

(b) Width change analysis of the outer magnetic yoke of electromagnetic actuator for spring-structure

Fig. 12. (Color online) The width change analysis of the outer magnetic yoke of electromagnetic actuator.

static iron core is significantly reduced due to magnetic saturation. Fig. 12(b) shows that when the outer yoke width is increased by 0.45 mm and decreased by 0.45 mm, the suction force generated by the moving and static iron core slightly changes.

3.4. Electromagnetic actuator Matlab and Adams joint simulation analysis

Fig. 13 shows the joint simulation model of the PM structure electromagnetic actuator. Fig. 13(a) shows the electromagnetic actuator Matlab and Adams joint simulation model. Fig. 13(b) shows the electromagnetic actuator Adams simulation interface model. F_1 is the closing handle thrust. F_3 is the bearing torsion spring pressure. F is thrust that the moving ejector pin breaking the main contact. x is the displacement between the moving and static iron cores. The model detects the displacement x in real time. When x is $0 < x < 3$, the main circuit is closed with the switch B1, and the miniature circuit breaker works for the main circuit. When x is $3 \le x \le 5.2$, the main circuit is closed to B2, and the miniature circuit breaker is switched to the auxiliary circuit. The two-dimensional real-time look-up table is used to obtain the ejector pin thrust of the moving iron core to disconnect the main contact, and the joint simulation of the electro-

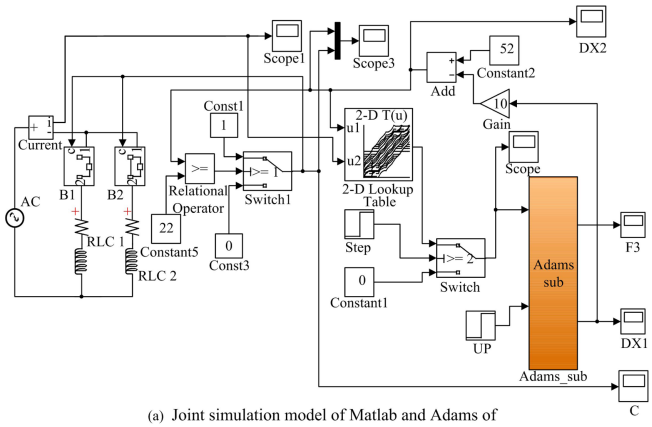

(a) Joint simulation model of Matlab and Adams of the electromagnetic actuator

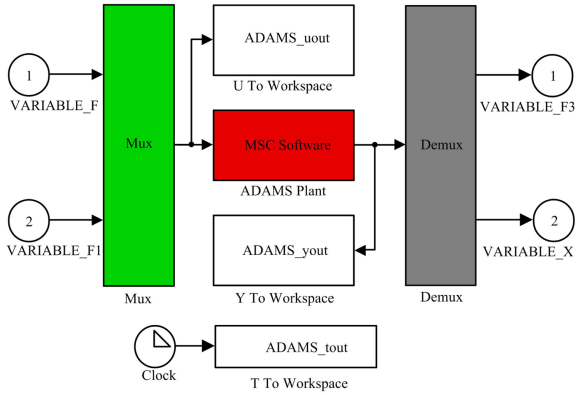

(b) Adams simulation interface model of the electromagnetic actuator

Fig. 13. (Color online) Co-simulation model of electromagnetic actuator for PM structure.

magnetic actuator motion process by Matlab and Adams is realized. By continuously adjusting the parameters of the joint simulation model, the structural design parameters of the electromagnetic actuator are continuously adjusted. The displacement of the electromagnetic actuator simulation model of the spring-structure is 7.7 mm, and the simulation method is the same as the electromagnetic actuator joint simulation method of the PM structure.

For the rigid body i of the electromagnetic actuator in Adams, the Cartesian (x, y, z) coordinates of the centroid in the inertial reference frame and the Euler angle (ψ, θ, φ) reflecting the orientation of the rigid body are used as generalized coordinates, i.e.

$$\boldsymbol{q}_i = [x, y, z, \psi, \theta, \varphi]_i^T \tag{11}$$

Where $\boldsymbol{q}$ is system generalized coordinate array; $\boldsymbol{q} = [\boldsymbol{q}_1^T, \boldsymbol{q}_2^T, \ldots, \boldsymbol{q}_n^T]$.

Each rigid body is described by six generalized coordinates. According to the Lagrange multiplier method, the multi-rigid system dynamics equation is

$$\begin{cases} \dfrac{d}{dt}\left(\dfrac{\partial \boldsymbol{T}}{\partial \dot{\boldsymbol{q}}}\right)^T - \left(\dfrac{\partial \boldsymbol{T}}{\partial \boldsymbol{q}}\right)^T + \boldsymbol{\psi}_q^T \boldsymbol{\rho} + \boldsymbol{\theta}_{\dot{q}}^T \boldsymbol{u} = \boldsymbol{Q} \\ \boldsymbol{\psi}(\boldsymbol{q}, t) = 0 \\ \boldsymbol{\theta}(\boldsymbol{q}, \dot{\boldsymbol{q}}, t) = 0 \end{cases} \tag{12}$$

Where $\boldsymbol{T}$ is system energy; $\boldsymbol{Q}$ is generalized force array; $\boldsymbol{\psi}_q$ is complete constraint of x axis rotation; $\boldsymbol{\rho}$ is Lagrangian multiplier array corresponding to the complete constraint; $\boldsymbol{u}$ is Lagrangian multiplier array corresponding to non-holonomic constraint; $\boldsymbol{\psi}(\boldsymbol{q}, \mathrm{t}) = 0$ is a complete constraint equation; $\boldsymbol{\theta}(\boldsymbol{q}, \dot{\boldsymbol{q}}, \mathrm{t}) = 0$ is a non-holonomic constraint equation.

The rigidity coefficient of the bearing torsion spring is set, as per the following formula.

$$T = \frac{E \times d^4}{3667 \times D \times n} \tag{13}$$

Where d is diameter of the bearing torsion spring wire, with the value of 0.8 mm; D is the medium diameter of the bearing torsion spring coil, with the value of 2.8 mm; n is the number of turns of the bearing torsion spring, with the value of 4; and E is the modulus of elasticity. In this design, take carbon steel wire as the bearing torsion spring material, and set $E = 206 \times 10^3$ MPa.

After modeling in UG8.0, the model is imported into Adams software, combined with the control circuit model of Matlab/Simulink of Fig. 13. As per the joint simulation model of Adams and Matlab, perform the dynamic simulation of the whole process for the PM and spring structure miniature circuit breaker electromagnetic actuator. Fig. 14 shows the SMCB electromagnetic actuator Adams simulation model. Fig. 14(a) shows the PM structure electromagnetic actuator Adams simulation model; Fig. 14(b) shows the spring-structure electromagnetic actuator Adams simulation.

Fig. 15 shows the co-simulated results of the torsion spring pressure for the bearing torsion spring of the miniature circuit breaker PM and spring-structure electromagnetic actuator. Fig. 15(a) is the simulation result of the torsion spring pressure for the PM structure electromagnetic actuator bearing torsion spring, and Fig. 15(b) is for the spring-structure. Fig. 15(a) shows that the initial torsion spring pressure of the PM structure bearing torsion is 21.6 N. When the moving ejector pin is at the maximum position, the torsion spring pressure for the bearing torsion spring

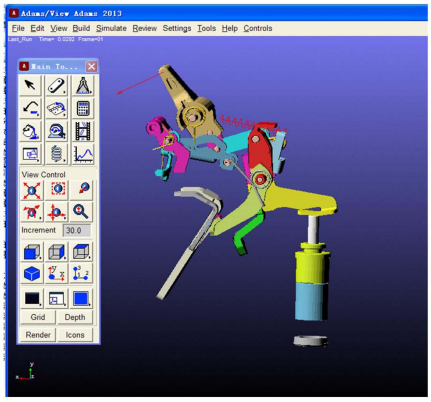

(a) Adams simulation model of electromagnetic actuator for PM structure

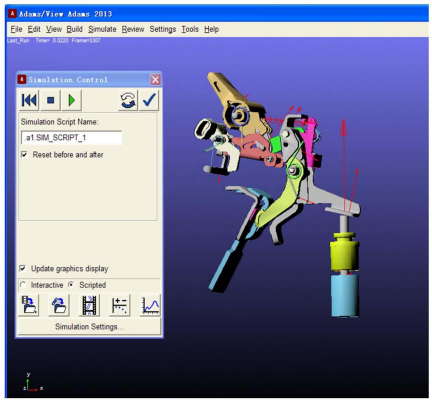

(b) Adams simulation model of electromagnetic actuator for spring-structure

Fig. 14. (Color online) Adams simulation model of electromagnetic actuator.

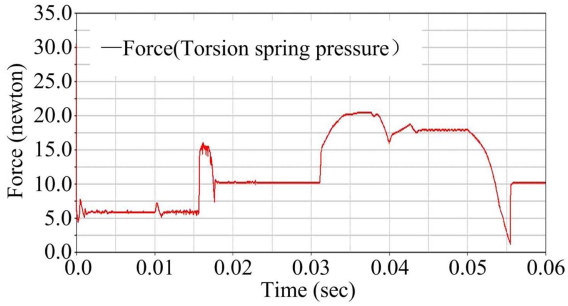

(a) Simulation result of the torsion spring pressure of the bearing torsion spring for the PM structure

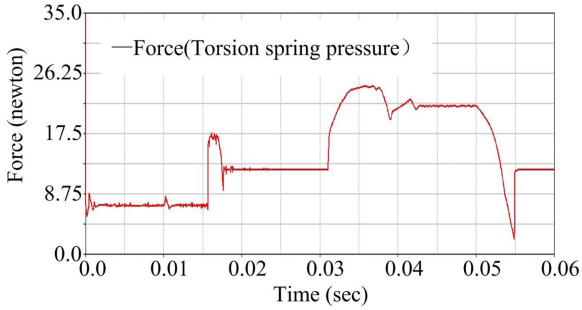

(b) Simulation result of the torsion spring pressure of the bearing torsion spring for the spring-structure

Fig. 15. (Color online) The torsion spring tension co-simulation simulation result of bearing torsion spring for electromagnetic actuator.

is 17.8 N. Fig. 15(b) shows that the initial torsion spring pressure of the spring-structure bearing torsion is 24.1 N. When the moving ejector pin is at the maximum position, the torsion spring pressure for the bearing torsion spring is 21.5 N. The initial torsion spring pressure for the bearing torsion spring is large, and the initial jacking force of the electromagnetic actuator is increased. When the moving ejector pin detach the main contact to the maximum position, the torsion spring pressure for the bearing torsion spring excessively increases the retention, which may cause a short-circuit short-delay failure. In addition, the spring reaction force of the spring-structure is gradually increased relative to the process in which the reaction force of the PM is gradually reduced. During the operation of the moving ejector pin, the electromagnetic force generated by the electromagnetic coil acting on the moving iron core is still necessary to overcome the large spring reaction force and detach the main contact. This is not good to quickly detach the miniature circuit breaker main contact. Based on this, the PM structure electromagnetic actuator is selected when design SMCB.

4. Electromagnetic Actuator Structural Optimized Design

4.1. Selection of optimization variables

The preliminary design parameters of the electromagnetic actuator are obtained by adjusting the Adams dynamics simulation of the electromagnetic actuator parameters. In order to achieve the electromagnetic actuator optimal output characteristics, it is necessary to optimize the structural parameters. The five key size parameters in the structural model shown in Fig. 3(a) are selected as optimization variables.

$$X = [h_2, h_3, h_4, r_2, r_3] \tag{14}$$

Where h_2, h_3, h_4, r_2, r_3 are the height of the moving iron core, height of the static iron core, height of the static iron core lower yoke, radius of the moving iron core and the static iron core. Given the moving iron core installation position limit, the moving iron core height is set to vary between 13.6 mm and 16.6 mm, and the size range of the remaining optimization variables is set to ± 20% of the initial design size.

4.2. Objective function

Given the installation space limitation, it requires small volume of the electromagnetic actuator, as large collision energy of the moving iron core may cause the rebound of the moving ejector pin. Select the electromagnetic actuator volume V and the moving iron core moving speed v as the objective function of the optimized design.

$$minf(X) = [V, v] \tag{15}$$

In formula (15), the electromagnetic actuator volume V can be expressed as

$$V = \pi r_2^2 (h_2 + h_3 + h_4) \tag{16}$$

The quantum particle swarm optimization algorithm is used to construct the fitness calculation function as

$$Y = V + v \tag{17}$$

4.3. Dynamic motion process mathematical model

The SMCB electromagnetic actuator dynamic differential equation of the motion process is

$$\begin{cases} \dfrac{d\psi}{dt} = U_m \sin(\omega t + \varphi) - iR \\ \dfrac{dv}{dt} = \dfrac{F_a - F_r}{m} \\ v = \dfrac{dx}{dt} \\ m = \rho \cdot \pi \cdot r_2^2 \cdot h_2 \\ R = \begin{cases} 0.368\Omega \cdots\cdots 0 < x < 3mm \\ 0.688\Omega \cdots\cdots 3mm \le x \le 5.2mm \end{cases} \\ F_f = \begin{cases} F_f \cdots\cdots\cdots\cdots\cdots\cdots\cdots\cdots\cdots\cdots 0 < x < 1.2mm \\ F_f + \dfrac{1.8 \cdot \left[1 + 7 \cdot \dfrac{x - 1.2}{5.1 - 1.2}\right] + 90}{5.5} \cdots 1.2mm \le x \le 5.2mm \end{cases} \\ \psi\big|_{t=0} = 1.03 \cdot 10^{-4} wb, \varphi = \dfrac{\pi}{2.4}, v\big|_{t=0} = 0, x\big|_{t=0} = 3 \cdot 10^{-4} m \\ \Delta t = 10^{-6}, \rho = 7900 kg/m^3 \end{cases} \tag{18}$$

Where ψ is the electromagnetic coil flux linkage; U_m is the power supply voltage amplitude; ω is the power supply angular frequency; φ is the closing phase angle; i is the electromagnetic coil current; R is the coil resistance, when the main circuit is working, $R = 0.368\Omega$, and when switching to the auxiliary circuit, $R = 0.688\Omega$; v is the speed of the moving iron core; F_a, F_r is the electromagnetic attraction and reaction force; F_f is the PM suction force to the moving iron core at the initial position; m is the moving iron core mass; ρ is the iron density; Δt is the time interval.

4.4. Quantum particle swarm optimization

The expression of quantum particle swarm is

$$\begin{cases} q_{i,j}(t) = \varphi_{i,j}(t) P_{i,j}(t) + (1 - \varphi_{i,j}(t)) G_j(t) \\ a(t) = \dfrac{1}{n} \left(\sum_{i=1}^{n} P_{i,1}(t), \sum_{i=1}^{n} P_{i,2}(t), \ldots, \sum_{i=1}^{n} P_{i,m}(t)\right) \\ x_{i,j}(t+1) = q_{i,j}(t) \pm \theta \left| a_j(t) - x_{i,j}(t) \right| \ln\left(\dfrac{1}{u_{i,j}(t)}\right) \\ i = 1 \ldots n, j = 1 \ldots m \end{cases} \tag{19}$$

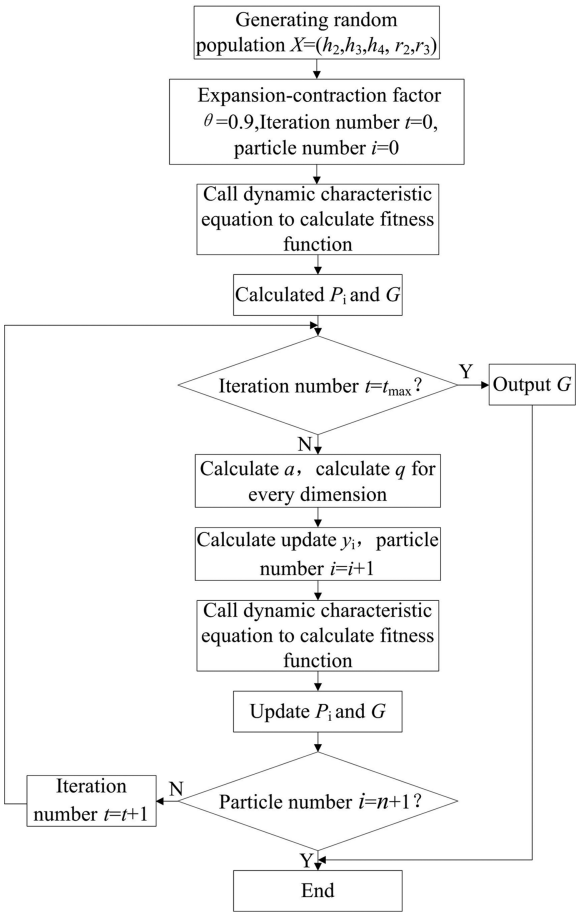

Fig. 16. Optimization control flow for electromagnetic actuator of quantum particle swarm algorithm.

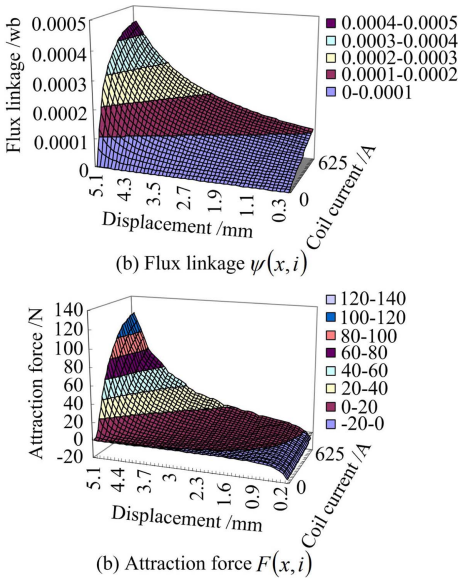

Fig. 17. (Color online) The change curve of flux and attraction.

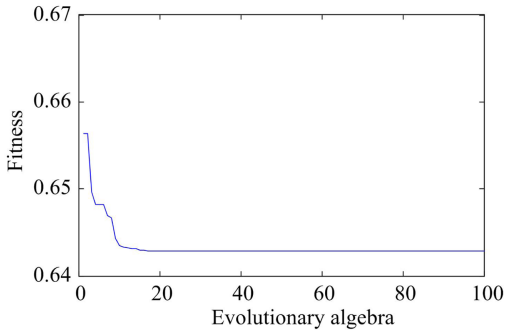

Fig. 18. (Color online) Optimization iterative relationship of the optimal individual fitness.

Where t is the number of iterations of the algorithm; φ, u is a random number between 0 and 1; P_i is the individual with the best fitness of particle i in the particle swarm iterative process; G is the best fit of n P particles; q is the attractor; a is the best position of the average; n is the number of particle for the particle swarm; m is the dimension of the particle x; when $u_{i,j}(t) \le 0.5$, take positive sign before θ, otherwise, take negative sign; θ is an expansion-contraction factor.

The electromagnetic actuator optimization control flow of the quantum particle swarm algorithm is shown in Fig. 16. In the optimization of the dynamic characteristics of the electromagnetic actuator, Ansys is first used to calculate the two-dimensional static data grid of the magnetic link $\psi(x,i)$ and electromagnetic force $F(x,i)$ under different coil currents and moving iron core displacements. The Runge-kutta iterative method is used to solve the dynamic process quickly.

Fig. 17 shows the electromagnetic relationship curves of the flux linkage $\psi(x,i)$ and suction force $F(x,i)$ under different coil currents and moving iron core displacements for electromagnetic actuator initial structure design.

Set the number of particle populations to 40 and the maximum iteration number t to 100. Each component of the initialization particle x is randomly distributed within its range of values. The quantum particle swarm optimization algorithm is called to optimize 10 times, and the optimal solution is obtained with h_2 = 16.6 mm, h_3 = 5.84 mm, h_4 = 1.2 mm, r_2 = r_3 = 3.68 mm, and the relationship between the fitness of the optimal particle G and the number of optimizations in the optimization process is shown in Fig. 18. As the optimization process proceeds, the value of the optimization function is continuously decreasing, thereby achieving the optimization goal of the minimum collision energy while minimizing the volume of the electromagnetic actuator.

4.5. Electromagnetic actuator structural optimization results

Set the electromagnetic actuator of the SMCB with

Table 1. Optimization results of main parameters for electromagnetic actuator.

	Parameter	Before optimization	After optimization
Parameter variable	Moving iron core height h_2 (mm)	13.6	16.6
	Static iron core height h_3 (mm)	7.3	5.84
	Static iron core lower yoke h_4 (mm)	1.5	1.2
	Moving iron core radius r_2 (mm)	4.6	3.68
	Static iron core radius r_3 (mm)	4.6	3.68
Optimization objective	Electromagnetic actuator volume V (mm^3)	1488.3	1005.2

rated current of 100A as optimized design object. The quantum particle swarm optimization algorithm is used to optimize the parameters of the electromagnetic actuator. The optimization results of the electromagnetic actuator main parameters are shown in Table 1. It can be seen from the Table 1 that the height of the moving iron core is increased to 16.6 mm, compared to pre-optimized 13.6 mm. The height of the static iron core is reduced to 5.84 mm, compared to pre-optimized 7.3 mm. The height of the lower yoke of the static iron core is reduced to 1.2 mm, compared to pre-optimized 1.5 mm. The optimized height of the moving and static iron cores, the lower yoke height of the static iron core can reduce the magnetic flux leakage between the moving and static iron cores and the support brackets of the outer yoke. It ensures that the suction characteristics between the moving and static iron core increase gradually under the electromagnetic actuator motion process. The radius of the moving and static iron core are reduced to 3.68 mm, compared to pre-optimized 4.6 mm, which ensures the action threshold point and instantaneous output characteristics between the PM and the moving iron core under E and C_S characteristics. The volume of the electromagnetic actuator is reduced to 1005.2 mm^3, compared to pre-optimized 1488.3 mm^3, which realizes the short-circuit short-delay characteristic of SMCB and reduces the installation volume of the electromagnetic actuator.

4.6. Experimental analysis of miniature circuit breaker

The experimental test was performed on the electromagnetic actuator of the miniature circuit breaker with

Table 2. Experiment and simulation results of electromagnetic actuator before and after optimization.

Position	Initial design structure		Optimized structure	
	Simulation average value (N)	Experimental test average value (N)	Simulation average value (N)	Experimental test average value (N)
A	4.7	4.5	5.5	5.2
B	10	9.5	7	6.5
C	8	7.8	3.5	3.5

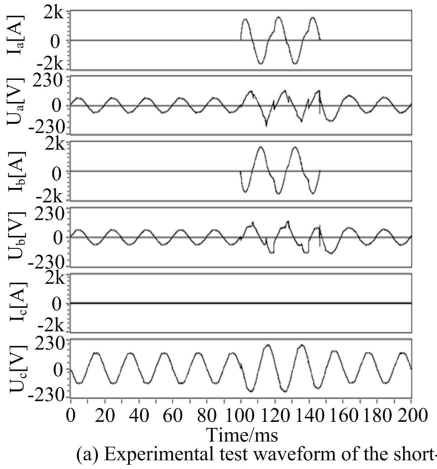

(a) Experimental test waveform of the short-circuit current

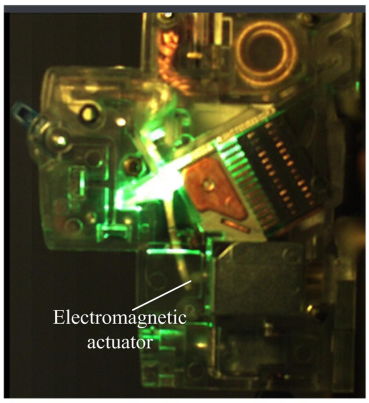

(b) High-speed photographic image of electromagnetic actuator under the initial jacking force

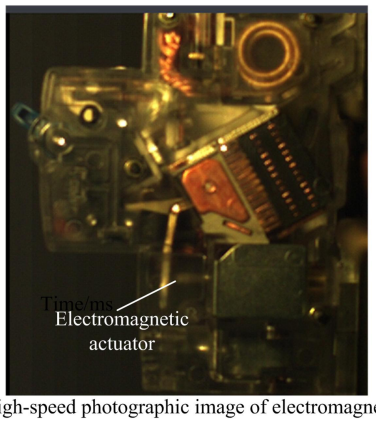

(c) High-speed photographic image of electromagnetic actuator under the retention force

Fig. 19. (Color online) Test platform of short-circuit current.

rated current of 100A. The hole was drilled at the position of the ejector rod action point. The test was performed by using a 10 N spring scale, with 10 times for mean value. Table 2 shows the experimental and simulation results of the electromagnetic actuator prior and post the optimization of the test. A is the position when the moving contact and the static contact are just separated. B is the middle position of the moving contact during the movement. C is the maximum position from the moving contact to opening distance. The table shows that the optimized initial jacking force of the electromagnetic actuator is 5.2 N, and the retention of the electromagnetic actuator pushing to the maximum position is 3.5 N, which achieves the expected optimization effect.

At the same time, short-circuit experimental test was performed on the designed 100A miniature circuit breaker under rated voltage $U_e = 230$ V, short-circuit current I = 1000A, power factor $\cos\theta = 0.980$ and test type O. The test platform is shown in Fig. 19. Fig. 19(a) shows the experimental test waveform of the short-circuit current, and Fig. 19(b) shows the high-speed photographic image of electromagnetic actuator under the initial jacking force, Fig. 19(c) shows the high-speed photographic image of electromagnetic actuator under the retention force. The photographic image shows that, the current peak value is $(I_p)\mathrm{a} = 1326.3\mathrm{A}$, $(I_p)\mathrm{b} = 1342.0\mathrm{A}$, $(I_p)\mathrm{c} = 17.2\mathrm{A}$, the on-off time is T_{mb} = 46.3 ms and the arcing time is T_{arc} = 9.8 ms. The electromagnetic actuator instantaneously drives the moving ejector pin to push the main contact, so that the contact is quickly detached. The arc generated by the main contact is momentarily very large under the initial jacking force. When the maximum position is reached, it is better to maintain the maximum position and achieve the purpose of selective protection.

5. Conclusions

Based on the working performance of SMCB electromagnetic actuator, this paper first analyzes the principle of the action threshold point and the output force characteristic of the E and C_S characteristics of the short-delay trip mechanism. Then, it analyzes the magnetic field distribution and suction characteristics of the PM structure and the spring-structure electromagnetic actuator in different topologies via Ansys software. Merge the mathematical model in electric circuit and magnetic circuit, and establish the joint simulation platform of Matlab and Adams. Simulate and analyze the force energy characteristics in the different electromagnetic actuators, and establish the PM mechanism topology structural model. Perform the dynamic optimization design of the 100A miniature circuit breaker electromagnetic actuator, based on the quantum particle swarm optimization algorithm. Finally, design a SMCB prototype with 100A rated current and build the experimental platform. The initial jacking force of the electromagnetic actuator is increased to 5.2 N, compared to pre-optimized 4.5 N. The retention is reduced to 3.5 N, compared to pre-optimized 7.8 N. When short circuit experimental current reaches 1000A, the electromagnetic actuator instantaneously drives the moving ejector pin to detach the main contact for the maximum position retention. Thus, it implements short-circuit short-delay characteristic in a good mechanism.

Acknowledgment

This work was supported by the National Natural Science Foundation of China under Grant 51307011, the Natural Science Research Key Project of the Anhui Higher Education Institutions of China under Grant KJ2016A528.

References

[1] D. Z. Xiong, X. Q. Chen, J. Yang, Y. Xue, and P. H. Zhang, Trans. Chin. Electrotech. Soc. **34**, 2333 (2019).
[2] H. Gong and M. Zong, Proc. In 7th Int. Conf. on Electron. and Info. Eng., Nanjing, China, 691 (2016).
[3] C. Rümpler, H. Stammberger, and A. Zacharias, In Proc. 57th IEEE Holm Conf. Elect. Contacts, Minneapolis, MN, USA, 1 (2011).
[4] L. Ji, D. G. Chen, and Y. Y. Liu, Proc. Chin. Soc. Electrical Eng. **29**, 107 (2009).
[5] C. Franck, IEEE Trans. Power Del. **26**, 998 (2011).
[6] Q. Yang, M. Z. Rong, and Y. Wu, Proc. Chin. Soc. Electrical Eng. **27**, 84 (2007).
[7] Y. Zhou and Z. L. Ye, Low Vol. App. **2**, 20 (2012).
[8] Y. Wu, M. Z. Rong, and Y. Fei, IEEE Trans. Plasma Sci. **39**, 2858 (2011).
[9] M. Z. Rong, Y. Fei, and Y. Wu, IEEE Trans. Plasma Sci. **38**, 2306 (2010).
[10] L. Liu, X. Y. Chen, and T. T. Qi, Proc. Chin. Soc. U. Electric Power Sys. Automat. **28**, 69 (2016).
[11] L. Ji, D. Chen, Y. Liu, and X. Li, IEEE Trans. Power Del. **26**, 222 (2011).
[12] Q. Wang, X. W. Li, and D. G. Chen, IEEE Trans. Com. Packag. Technolo. **4**, 1177 (2014).
[13] J. C. Gong, K. Huang, and H. Xue, Low Vol. App. **4**, 50 (2013).
[14] G. F. Ding, H. Xue, and H. Zhao, Low Vol. App. **1**, 51 (2010).
[15] K. J. Lu and P. B. Yan, Low Vol. App. **6**, 18 (2014).